

Journal Name

Crossmark

PAPER

RECEIVED
dd Month yyyy
REVISED
dd Month yyyy

Equation of state of QCD(-like) theory using Lattice Monte Carlo simulations

Etsuko Itou^{1,2}

¹Yukawa Institute for Theoretical Physics, Kyoto University, Kitashirakawa Oiwakecho, Sakyo-ku, Kyoto 606-8502, Japan ²Interdisciplinary Theoretical and Mathematical Sciences Program (iTHEMS), RIKEN, Wako, Saitama 351-0198, Japan

E-mail: itou@yukawa.kyoto-u.ac.jp**Keywords:** lattice QCD, finite density, two-colour QCD, equation of state, sound velocity, neutron stars**Abstract**

The equation of state (EoS) of strongly interacting matter at low temperature and high baryon density is a central ingredient in the physics of compact stars, but it is still difficult to determine directly from first-principles QCD calculations because of the sign problem. Two-colour QCD (QC₂D) provides a useful and controllable laboratory: for an even number of fundamental flavours the fermion determinant is real and positive, while the theory shares the nonperturbative properties with three-colour QCD at least zero chemical-potential regime. In this short review we summarize recent lattice progress on dense QC₂D, with emphasis on the phase structure, the emergence of superfluidity, the Bose–Einstein-condensation (BEC) to Bardeen–Cooper–Schrieffer (BCS) crossover, and thermodynamic quantities. A particularly interesting outcome is that the sound velocity in the cold dense superfluid regime can exceed the conformal value $c_s^2/c^2 = 1/3$. This behaviour, now seen in the simulations for several QCD-like theories, gives a stiff strongly interacting matter. It is expected to offer insight into at least some aspects of the physics realized inside neutron stars.

1 Introduction

Lattice QCD has become a quantitatively reliable nonperturbative method for the vacuum and finite-temperature regimes of strong interactions. The hadron spectrum and the chiral crossover temperature are now known with high precision from simulations with dynamical quarks, and the thermal equation of state (EoS) has also been determined precisely [1, 2]. In particular, the thermal EoS provides the energy density and pressure that enter the energy–momentum tensor in the Friedmann equations used to describe the evolution of the Universe. The situation is much less satisfactory in the cold and dense region. Once a quark chemical potential μ is introduced, the Euclidean Dirac determinant becomes complex in three-colour QCD, and ordinary importance sampling methods cannot be applied. This is the well-known sign problem; in its generic form, it is known to be NP-hard ¹, and its computational cost is expected to grow rapidly toward the thermodynamic limit [3, 4, 5].

There are nevertheless QCD-like theories in which dense matter can be studied directly. The most popular examples are QCD with isospin chemical potential and two-colour QCD (QC₂D). In the latter theory, the pseudo-reality of the fundamental representation of SU(2) makes the fermion determinant real, and for an even number of flavours it becomes positive. Therefore Hybrid Monte Carlo simulations based on the importance sampling method can be performed. QC₂D is not real-world QCD: its baryons are bosonic diquarks, and the superfluid condensate is a colour singlet. Even so, it is a valuable testing ground because it shares confinement, chiral symmetry breaking and asymptotic freedom with ordinary QCD at least zero chemical potential regime.

Among the quantities that can be studied in dense QCD-like theories, the EoS and the sound velocity are of particular interest. They are also directly connected to current questions in compact-star physics: neutron-star observations, through masses and radii relation, constrain the

¹Here, NP (nondeterministic polynomial time) denotes the complexity class of decision problems for which a proposed answer can be verified in polynomial time. NP-hard means that the problem is at least as hard as any problem in NP.

EoS of cold dense matter, and many phenomenological analyses suggest that the speed of sound may become large inside massive neutron stars [6, 7, 8, 9]. On the other hands, a reference value so-called the conformal bound,

$$c_s^2/c^2 = \frac{1}{3}, \quad (1)$$

has been discussed in some holographic models [10, 11]. Thus, the sound velocity has an upper bound, which is the value at an ideal relativistic gas. Lattice results for QCD and QCD-like theories at least at finite temperatures has not shown any violation of this value (see e.g. Refs. [1, 2]). Whether it is a true bound in cold dense QCD remains unknown, and recent results in sign-problem-free QCD-like theories provide a useful arena to address this question.

This review is organized as follows. Section 2 summarizes the lattice formulation used in our series of QC₂D studies. Section 3 reviews the phase structure, including the hadronic phase, the superfluid phase, the BEC–BCS crossover and gluonic observables. Section 4 discusses the EoS and the sound velocity. Section 5 gives summary and outlook.

2 Two-colour QCD on the lattice

2.1 QC₂D lattice action to study cold and dense regime

The Lagrangian here we consider is given by

$$\mathcal{L} = -\frac{1}{4}F_{\mu\nu}^a F_{\mu\nu}^a + \bar{\psi}(i\gamma_\mu D_\mu + m)\psi + \mu\bar{\psi}\gamma_0\psi - j[\bar{\psi}_1(C\gamma_5)\tau_2\bar{\psi}_2^T - \psi_2^T(C\gamma_5)\tau_2\psi_1], \quad (2)$$

in the continuum limit. We mainly consider two-flavour QC₂D in this manuscript. The first two terms are the same as those in the standard QCD Lagrangian, and the third term is the density term associated with the quark number operator. The term proportional to j is the diquark source term, which explicitly breaks the $U(1)_B$ symmetry. In a finite volume, such an explicit breaking term is introduced to study the spontaneous breaking of $U(1)_B$ through the diquark condensate, and the physical result is obtained by taking the $j \rightarrow 0$ limit.

In the lattice simulations, we use the Iwasaki gauge action and two flavours of Wilson fermions [12, 13, 14, 15]. The action for quarks is expressed by

$$S_F = \bar{\psi}_1\Delta(\mu)\psi_1 + \bar{\psi}_2\Delta(\mu)\psi_2 - J\bar{\psi}_1(C\gamma_5)\tau_2\bar{\psi}_2^T + J\psi_2^T(C\gamma_5)\tau_2\psi_1, \quad (3)$$

where $\Delta(\mu)$ denotes the Wilson–Dirac operator includes the density term. The diquark source parameter j becomes $J = j\kappa$, where κ denotes the hopping parameter coming from the normalization of the Wilson fermion on the lattice. For $SU(2)$ gauge fields, the link variable satisfies $U_\mu^* = \tau_2 U_\mu \tau_2$. The Dirac operator then obeys

$$\Delta(\mu)^* = \tau_2(C\gamma_5)\Delta(\mu)(C\gamma_5)^{-1}\tau_2, \quad (4)$$

and hence $\det \Delta(\mu)$ is real. Furthermore, the fermion action, Eq. (3), takes positive if we consider two degenerate masses for flavours. This is the reason why even-flavor dense QC₂D can be simulated by standard Monte Carlo methods.

The absence of the sign problem is not the whole story. Around the onset scale $\mu \simeq m_{PS}/2$, where m_{PS} denotes the mass of the pseudo-scalar meson (pion) at $\mu = 0$, numerical instabilities arise coming from the emergence of the zero eigenvalue of the Wilson–Dirac operator [16, 17]. This numerical instability can be controlled by introducing a small diquark source term proportional to J . Technically, this source lifts the eigenvalues of the Wilson–Dirac operator, thereby stabilizing the simulation. In Monte Carlo simulations, the fermionic degrees of freedom are integrated out analytically, leaving the action written only in terms of the gauge fields. The presence of the diquark source term requires a corresponding modification of this Gaussian integration. The fermion action is therefore rewritten with an extended matrix, and Rational Hybrid Monte Carlo is used for the two-flavour theory (see detail Ref. [12, 15]).

The numerical results reviewed here were obtained at $(\beta, \kappa) = (0.800, 0.159)$. The relative scale setting was obtained from the gradient-flow scale w_0 and the pseudocritical temperature at $\mu = 0$ [13]. With the convention $T_c \simeq 200$ MeV, the lattice spacing is approximately $a = 0.17$ fm, and the pseudoscalar mass is $m_{PS} \simeq 738$ MeV. The low-temperature data have been obtained on 16^4 and 32^4 lattices, corresponding roughly to $T \simeq 80$ MeV and $T \simeq 40$ MeV, respectively [12, 15].

The role of this scale setting should be kept in mind. Since QC₂D is not a theory of nature, there is no unique experimental quantity with which to set the absolute scale. The convention above is chosen so that temperatures and chemical potentials can be displayed in familiar units. The more robust quantities are dimensionless ratios such as T/T_c , μ/m_{PS} and m_{PS}/m_V . In

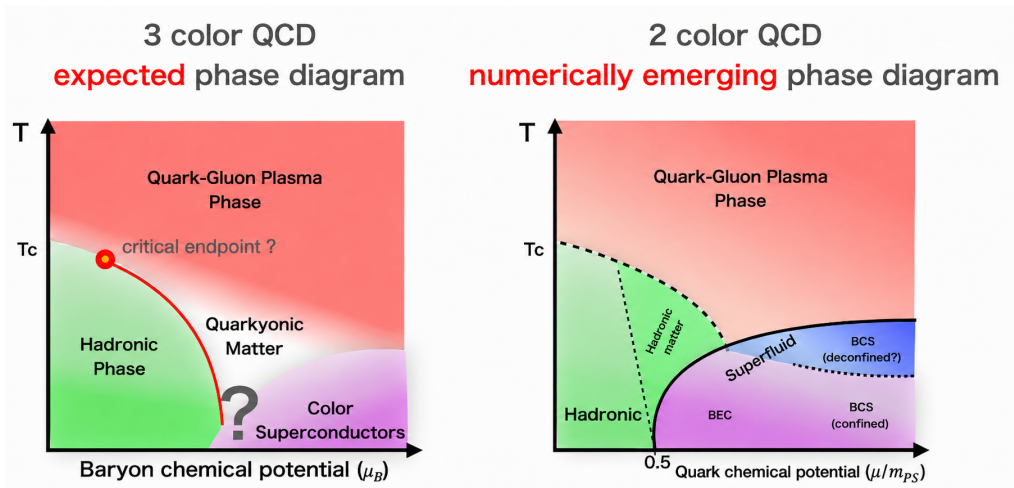


Figure 1. Schematic comparison of the phase diagrams of three-colour QCD and two-colour QCD. The three-colour QCD panel is based on the phase-diagram review of Fukushima and Hatsuda [19]; the QC₂D panel summarizes the lattice picture obtained in Ref. [15].

particular, the statement that the superfluid onset occurs at $\mu \simeq m_{\text{PS}}/2$ is independent of the arbitrary conversion to MeV.

There are two practical upper limits on the chemical potential. The first is the lattice saturation effect, in which all lattice sites become filled with quarks. The second, usually more restrictive in the parameter range of present simulations, is the appearance of large $a\mu$ artifacts before the saturation plateau is reached. In lattice simulations, the lattice spacing a provides the UV cutoff, and dimensionless quantities such as $a\mu$ should remain smaller than unity for reliable continuum-oriented physics. In our simulations, we indeed observed unphysical behaviour already around $a\mu \sim 0.8$, where quantities that should monotonically increase with μ started to decrease. In this review, we therefore do not consider the parameter region affected by such lattice artifacts from the physics discussion.

3 Phase structure

3.1 Observables

Before turning to the EoS, let us first look at the ground-state structure in the region of interest. Figure 1 shows a schematic comparison of the phase diagrams. The left panel shows the commonly expected phase structure of three-colour QCD, where the finite-baryon-density region is difficult to access directly from lattice simulations. The right panel shows the phase structure that has emerged from recent QC₂D simulations (See a recent review [18]). In the following, we introduce the physical observables used to distinguish these phases and give their definitions.

The Polyakov loop is used as a diagnostic of confinement,

$$L = \frac{1}{N_s^3} \sum_{\mathbf{x}} \text{tr} \prod_{\tau} U_4(\mathbf{x}, \tau). \quad (5)$$

The diquark condensate is the order parameter for the superfluid transition,

$$\langle qq \rangle = \frac{\kappa}{2} \langle \bar{\psi}_1 (C\gamma_5) \tau_2 \bar{\psi}_2^T - \psi_2^T (C\gamma_5) \tau_2 \psi_1 \rangle. \quad (6)$$

Also, the (net) quark number density,

$$a^3 \langle n_q \rangle = \sum_i \kappa \langle \bar{\psi}_i(x) (\gamma_4 - \mathbb{I}_4) e^{\mu} U_4(x) \psi_i(x + \hat{4}) + \bar{\psi}_i(x) (\gamma_4 + \mathbb{I}_4) e^{-\mu} U_4^\dagger(x - \hat{4}) \psi_i(x - \hat{4}) \rangle, \quad (7)$$

represents the difference between quark and antiquark densities and is used for identifying the crossover from the BEC-like regime to the BCS-like regime. The chiral condensate and the topological susceptibility are not used to define the phases in our terminology, but they provide important information about the vacuum structure at finite density.

Table 1 summarizes the definitions of these phases in terms of the behaviour of the corresponding observables. In this review, we mainly focus on the low-temperature region, with $T \approx 40$ MeV. In this region, the relevant phases are essentially the hadronic phase and the

Table 1. Definition of each phase of dense QC₂D. The BEC and BCS regimes are continuously connected inside the superfluid phase, but they are distinguished by the quantitative behaviour of the quark number density.

Regime	$\langle L \rangle$	$\langle qq \rangle$	$\langle n_q \rangle$
Hadronic	zero	zero	zero
Hadronic-matter	zero	zero	nonzero
BEC superfluid		nonzero	nonzero
BCS superfluid		nonzero	$\simeq n_q^{\text{tree}}$
QGP	nonzero	zero	nonzero

superfluid phase. Within the superfluid phase, there is also a crossover from a strongly coupled BEC regime to a weakly coupled BCS regime. This structure will be discussed below together with the numerical results.

Other possible phases include the hadronic-matter phase, which appears as a narrow region just below the superfluid transition at finite temperature below the pseudo-critical temperature (T_c). In this region, $\langle n_q \rangle$ is nonzero, while $\langle qq \rangle$ vanishes after the $J \rightarrow 0$ extrapolation. The region shrinks as the temperature is lowered, supporting the interpretation that it is generated by thermal excitations [12, 15]. In addition to these phases, at sufficiently high temperature, chiral symmetry is restored and deconfinement occurs, as in three-colour QCD, leading to the quark–gluon plasma (QGP) phase.

3.2 Hadronic-superfluid transition

The mean-field chiral perturbation theory (ChPT) prediction for QC₂D is that the superfluid transition occurs when the quark chemical potential reaches one half of the pseudo-scalar mass;

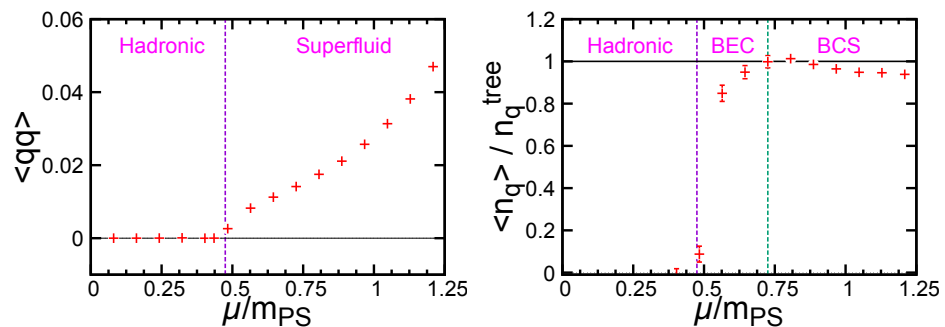
$$\mu_c \simeq \frac{m_{\text{PS}}}{2}. \quad (8)$$

According to the prediction [20], the diquark condensate behaves as

$$\langle qq \rangle = A(\mu - \mu_c)^{1/2}, \quad (9)$$

near the transition point. Lattice simulations with Wilson and staggered fermions have confirmed this picture at low temperature [12, 21, 22, 23, 24].

In our $T \simeq 40$ MeV study [15], we find the value of μ_c as $\mu_c/m_{\text{PS}} \simeq 0.48$ by fitting the data using Eq. (9). The resulting value is close to the expected value as shown in the left panel of Fig. 2. The quark number density (the right panel of Fig. 2) also turns on at approximately the same

**Figure 2.** Diquark condensate (Left panel) and quark number density (Right panel) as a function of the quark chemical potential in dense QC₂D at $T \simeq 40$ MeV. The data and analysis are taken from Ref. [15].

value. This provides evidence that a phase transition associated with the breaking of $U(1)_B$ occurs at this point.

3.3 BEC–BCS crossover

Inside the superfluid phase, there are at least two distinguished regimes; the BEC and BCS phases. Just above onset, tightly bound diquarks condense, and the analytic results from ChPT as an effective theory are expected to be reliable. At larger chemical potential, the typical distance between quarks decreases, and because of the asymptotic freedom of QCD(-like) theories, the relevant degrees of freedom become quarks near a Fermi surface; the system then becomes

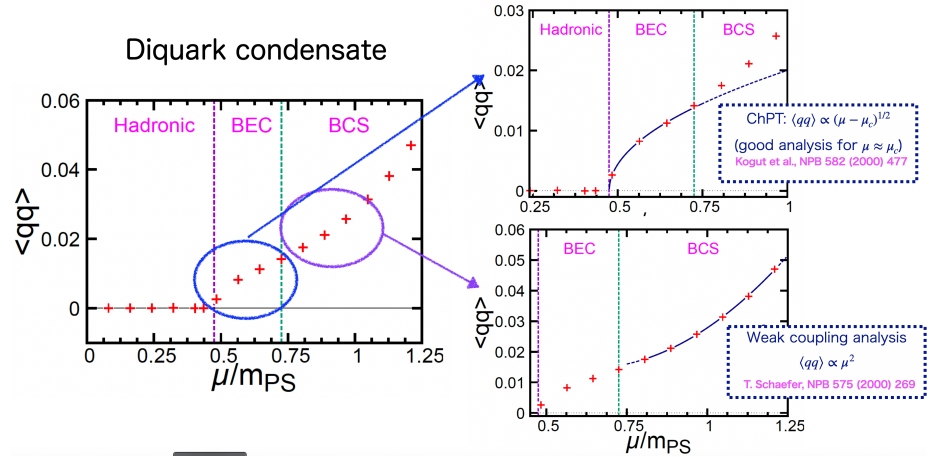


Figure 3. Scaling behaviour of the diquark condensate in dense QC₂D at $T \simeq 40$ MeV. In the BEC regime, the data are well described by the ChPT prediction, while in the BCS phase the condensate shows the approximate μ^2 scaling expected by the weak coupling analysis. The data and analysis are taken from Ref. [15].

BCS-like. Since the BEC–BCS change is a crossover rather than a symmetry-changing phase transition, its location is definition dependent.

A useful criterion is the ratio of the measured quark number density to the tree-level lattice density, n_q/n_q^{tree} [21]. Once this ratio approaches unity, the density is well described by weakly interacting quarks and the system is identified as BCS-like. The ratio reaches unity around $\mu/m_{PS} \simeq 0.73$ as shown in the right panel of Fig. 2.

The same region is also consistent with the weak-coupling expectation that the diquark condensate scales roughly as

$$\langle qq \rangle \propto \mu^2, \quad (10)$$

reflecting pairing near the Fermi surface [25, 26, 27]. On the other hand, in the BEC region the data of $\langle qq \rangle$ can be well fitted by the prediction of ChPT, Eq. (9). The enlarged plots for each region are shown in Fig. 3. Thus, the guideline for the BEC–BCS crossover determined from $\langle n_q \rangle$ also provides a consistent description of the change in the scaling behaviour of $\langle qq \rangle$, from the ChPT-like behaviour in the BEC regime to the weak coupling behaviour expected in the BCS regime.

3.4 Chiral condensate and gluonic observables

At high density, chiral symmetry is expected to be restored in both three-colour and two-colour QCD. Correspondingly, the chiral condensate decreases after the onset of superfluidity in several QC₂D simulations. In the BEC regime, the data in Ref. [15] follow the ChPT predictions,

$$\langle \bar{q}q \rangle(\mu) \propto \frac{1}{\mu^2}, \quad (11)$$

while at higher density it seems to become flatter at nonzero values. Because Wilson fermions explicitly break chiral symmetry, this behaviour should be interpreted carefully. Nevertheless, it indicates a tendency toward chiral-symmetry restoration. Recent studies have also shown that correlation functions of chiral partners become degenerate in the high-density region [28]. This provides further support for the tendency toward chiral restoration at high density.

The gluonic sector shows a different and quite interesting behaviour. Early studies discussed the possibility that the dense BCS regime might deconfine, but more recent work suggests that confinement can persist at low temperature even at large chemical potential. In a work of the static quark-antiquark potential, the potential remains linearly rising in the explored dense regime, and the string tension stays nonzero [29]. Independent Wilson and staggered studies also indicate that the deconfinement temperature remains of order 100 MeV at high density [22, 30].

The topological susceptibility provides another view of the same issue. At high temperature, where the Polyakov loop grows, topological fluctuations are suppressed as the chemical potential is increased. At low temperature, however, the simulations at $T \simeq 80$ MeV and $T \simeq 40$ MeV find an almost μ -independent topological susceptibility [12, 15]. This suggests that the cold dense regime retains nonperturbative gluonic features.

This separation between quark and gluon diagnostics is one of the central lessons of the present lattice results. In high-temperature QCD the chiral condensate, topological susceptibility and

Polyakov loop all change rapidly around the pseudo-critical temperature, giving a relatively coherent picture of the transition from hadrons to the QGP. In cold dense QC₂D, by contrast, the quark number density and diquark condensate indicate a weakly interacting quark picture, but the Polyakov loop, static potential and topology do not show the same kind of deconfining response. Thus, the BCS-like dense regime is not simply the low-temperature continuation of the high-temperature plasma.

4 EoS and sound velocity

4.1 Thermodynamic quantities

We now turn to the EoS and the sound velocity in the low-temperature regime discussed above, namely around $T \simeq 40$ MeV. The pressure at finite density is obtained from the quark number density by

$$p(\mu) - p(\mu_c) = \int_{\mu_c}^{\mu} n_q(\mu') d\mu', \quad (12)$$

in the thermodynamic limit. Here, $p(\mu) = 0$ in $\mu \leq \mu_c$. The trace anomaly is evaluated from derivatives of the lattice action with respect to the lattice spacing, which is explicitly given by

$$e - 3p = -\frac{T}{V} \left[a \frac{\partial \beta}{\partial a} \left\langle \frac{\partial S}{\partial \beta} \right\rangle + a \frac{\partial \kappa}{\partial a} \left\langle \frac{\partial S}{\partial \kappa} \right\rangle + a \frac{\partial j}{\partial a} \left\langle \frac{\partial S}{\partial j} \right\rangle \right]_{\text{sub}}, \quad (13)$$

where the subtraction removes the vacuum contribution. In present analyses, the first two terms are evaluated using the nonperturbative beta functions from the scale-setting study, while the last term is assumed to vanish in the $j \rightarrow 0$ limit. This assumption is plausible but should be checked more carefully in future work. Combining the pressure and the trace anomaly gives the internal energy density as a function of μ .

The resulting pressure and internal energy are shown in Fig. 4. These quantities grow rapidly

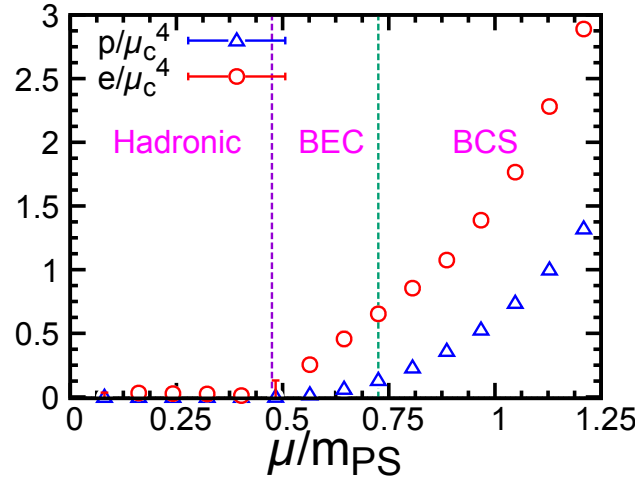


Figure 4. Pressure and internal energy density as functions of the quark chemical potential in dense QC₂D. The plot is originally obtained from the $T \simeq 40$ MeV lattice study of Ref. [15].

after the onset of superfluidity, while both p and e remain consistent with zero in the hadronic phase.

4.2 Sound velocity and conformal-bound violation

The sound velocity is then extracted from

$$c_s^2/c^2 = \left. \frac{\partial p}{\partial e} \right|_s \simeq \left. \frac{\partial p/\partial \mu}{\partial e/\partial \mu} \right|_T, \quad (14)$$

where the final expression is appropriate when thermal effects are small. The comparison of $T \simeq 80$ MeV and $T \simeq 40$ MeV data indicates that this approximation is reliable in the cold regime studied so far [14, 15]. The ChPT [31, 20, 21] predicts

$$(c_s^2/c^2)_{\text{ChPT}} = \frac{1 - \mu_c^4/\mu^4}{1 + 3\mu_c^4/\mu^4}. \quad (15)$$

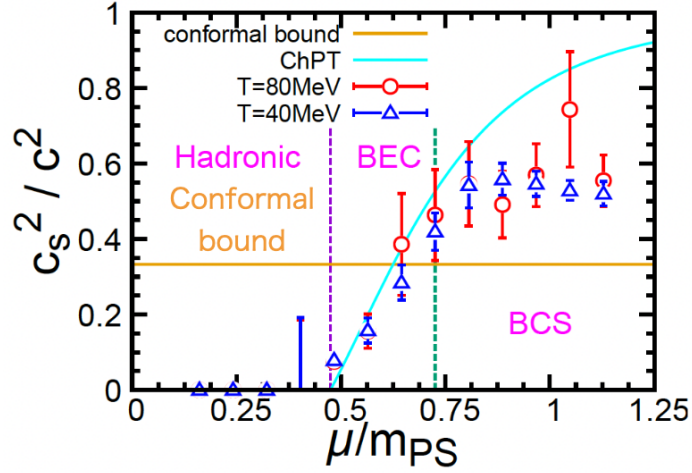


Figure 5. Squared sound velocity in dense QC₂D. The $T \simeq 80$ MeV result was first reported in Ref. [14], and the combined comparison with the $T \simeq 40$ MeV data was obtained in Ref. [15]. The horizontal orange line marks the conformal value $c_s^2/c^2 = 1/3$.

Figure 5 shows the sound velocity obtained from the simulations at $T \simeq 40$ MeV and $T \simeq 80$ MeV. The results at $T \simeq 40$ MeV and $T \simeq 80$ MeV show no difference within errors. In the hadronic phase, the sound velocity is consistent with zero, and it becomes nonzero after the transition to the superfluid phase. As in the cases of the diquark condensate and the chiral condensate, the data in the BEC regime agree well with the ChPT prediction, Eq. (15), shown by the cyan curve. Once the onset chemical potential μ_c is fixed, this ChPT prediction contains no free parameters, and the agreement provides a nontrivial check of the lattice calculation.

On the other hand, the ChPT expression gives $c_s^2/c^2 \rightarrow 1$ in the high-density limit, which is unphysical. Thus, the ChPT result should be regarded as applicable only near the onset of the superfluid phase. In the BCS-like regime, the lattice data deviate from the ChPT prediction and do not continue to increase as a function of μ . The important observation is that the sound velocity nevertheless exceeds the conformal value, $c_s^2/c^2 = 1/3$, in the BCS phase [14, 15]. Such behaviour had not been clearly observed in previous lattice calculations of QCD-like theories.

5 Conclusions and outlook

Dense two-colour QCD has developed into a quantitative laboratory for cold dense strong-interaction matter. The phase diagram is now rather coherent across independent simulations. The hadronic-superfluid transition occurs around $\mu_c \simeq m_{PS}/2$, the BEC–BCS crossover is visible through the quark number density and the diquark condensate. Furthermore, the low-temperature dense regime appears to retain confinement and unsuppressed topological fluctuations over the range explored so far.

The EoS gives the most provocative lesson. In the cold superfluid regime, lattice data show that the squared sound velocity can exceed the conformal value $1/3$. This result does not by itself solve the EoS of neutron-star matter, but it gives a first-principles demonstration that QCD-like dense matter can be stiff. It also sharpens the question of which features are universal among dense gauge theories and which rely on the special colour-singlet nature of the QC₂D diquark condensate.

Recent QC₂D work by other groups also reports a large sound velocity in the high-density regime [32]. Another sign-problem-free theory to dense matter is three-colour QCD at finite isospin chemical potential. In that case the chemical potentials of the up and down quarks have opposite signs, and the product of the two fermion determinants is real and positive. The onset to the superfluid phase can be controlled by charged pion condensation rather than by diquark condensation. An external pionic source is introduced to stabilize the numerical simulations in high-density regime, and observables are extrapolated to zero source. In such a QCD-like theory, the EoS and sound velocity have been studied without the baryon sign problem, and have shown the violations of the conformal value [33, 34, 35]

Real neutron-star matter is governed by three-colour QCD at baryon chemical potential, not by QC₂D. Therefore the lattice results reviewed here should not be inserted directly into astrophysical equations of state. Their value is instead conceptual: they provide a first-principles example of strongly interacting dense matter with a large sound velocity. This point is relevant because many

phenomenological analyses of neutron-star data favour a stiffening of matter at several times nuclear saturation density [7, 8, 9, 36]. Effective descriptions, including quarkyonic models, Nambu–Jona-Lasinio-type models, functional renormalization group studies and holographic constructions, have also found peaks in the sound velocity [37, 38, 39, 40].

The next steps are clear. Continuum and thermodynamic extrapolations are needed, especially for the sound velocity and gluonic observables. The chiral limit and lighter quark masses should be explored. More detailed comparisons among Wilson, staggered and improved actions will be essential. Finally, the relation between QC_2D , isospin-dense QCD and phenomenological dense QCD should be developed in a common language. These efforts will make sign-problem-free theories more useful as controlled laboratories for the physics of compact stars.

Acknowledgments

The author thanks K. Iida, K. Ishiguro, T.-G. Lee, K. Murakami and D. Suenaga for collaborations on the original works reviewed here. The author also thanks S. Hands, T. Hatsuda, T. Kojo, J.-I. Skullerud, N. Yamamoto for valuable discussions.

Funding

The author is supported by JSPS KAKENHI Grant Nos. 25K01001 and 23H05439, JST SQAI Grant No. JPMJPF2221, and JST CREST Grant No. JPMJCR24I3. This work is supported by the Program for Promoting Researches on the Supercomputer “Fugaku” (Simulation for basic science: from fundamental laws of particles to creation of nuclei; Simulation for basic science: approaching the new quantum era), and the Joint Institute for Computational Fundamental Science (JICFuS), Grant No. JPMXP1020230411. This work is supported by the Center for Gravitational Physics and Quantum Information (CGPQI) at the Yukawa Institute for Theoretical Physics.

Data availability

No new data were generated for this review.

References

- [1] Szabocls Borsanyi, Zoltan Fodor, Christian Hoelbling, Sandor D. Katz, Stefan Krieg, and Kalman K. Szabo. Full result for the QCD equation of state with 2+1 flavors. *Phys. Lett. B*, 730:99–104, 2014.
- [2] A. Bazavov et al. Equation of state in (2+1)-flavor QCD. *Phys. Rev. D*, 90:094503, 2014.
- [3] Matthias Troyer and Uwe-Jens Wiese. Computational complexity and fundamental limitations to fermionic quantum Monte Carlo simulations. *Phys. Rev. Lett.*, 94:170201, 2005.
- [4] Gert Aarts. Recent developments at finite density on the lattice. *PoS*, CPOD2014:012, 2015.
- [5] Keitaro Nagata. Finite-density lattice QCD and sign problem: Current status and open problems. *Prog. Part. Nucl. Phys.*, 127:103991, 2022.
- [6] Kota Masuda, Tetsuo Hatsuda, and Tatsuyuki Takatsuka. Hadron–quark crossover and massive hybrid stars. *PTEP*, 2013(7):073D01, 2013.
- [7] Gordon Baym, Tetsuo Hatsuda, Toru Kojo, Philip D. Powell, Yifan Song, and Tatsuyuki Takatsuka. From hadrons to quarks in neutron stars: a review. *Rept. Prog. Phys.*, 81(5):056902, 2018.
- [8] Sinan Altiparmak, Christian Ecker, and Luciano Rezzolla. On the Sound Speed in Neutron Stars. *Astrophys. J. Lett.*, 939(2):L34, 2022.
- [9] Len Brandes, Wolfram Weise, and Norbert Kaiser. Inference of the sound speed and related properties of neutron stars. *Phys. Rev. D*, 107(1):014011, 2023.
- [10] Paul M. Hohler and Mikhail A. Stephanov. Holography and the speed of sound at high temperatures. *Phys. Rev. D*, 80:066002, 2009.
- [11] Aleksey Cherman, Thomas D. Cohen, and Abhinav Nellore. A Bound on the speed of sound from holography. *Phys. Rev. D*, 80:066003, 2009.
- [12] Kei Iida, Etsuko Itou, and Tong-Gyu Lee. Two-colour QCD phases and the topology at low temperature and high density. *JHEP*, 01:181, 2020.

- [13] Kei Iida, Etsuko Itou, and Tong-Gyu Lee. Relative scale setting for two-color QCD with $N_f=2$ Wilson fermions. *PTEP*, 2021(1):013B05, 2021.
- [14] Kei Iida and Etsuko Itou. Velocity of sound beyond the high-density relativistic limit from lattice simulation of dense two-color QCD. *PTEP*, 2022(11):111B01, 2022.
- [15] Kei Iida, Etsuko Itou, Kotaro Murakami, and Daiki Suenaga. Lattice study on finite density QC₂D towards zero temperature. *JHEP*, 10:022, 2024.
- [16] S. Muroya, A. Nakamura, and C. Nonaka. Monte Carlo study of two color QCD with finite chemical potential: Status report of Wilson fermion simulation. *Nucl. Phys. B Proc. Suppl.*, 94:469–472, 2001.
- [17] Shin Muroya, Atsushi Nakamura, and Chiho Nonaka. Study of the finite density state based on SU(2) lattice QCD. *Nucl. Phys. B Proc. Suppl.*, 119:544–546, 2003.
- [18] Etsuko Itou. Lattice Results for the Equation of State in Dense QCD-like Theories. *Universe*, 11(11):380, 2025.
- [19] Kenji Fukushima and Tetsuo Hatsuda. The phase diagram of dense QCD. *Rept. Prog. Phys.*, 74:014001, 2011.
- [20] J. B. Kogut, Misha A. Stephanov, D. Toublan, J. J. M. Verbaarschot, and A. Zhitnitsky. QCD - like theories at finite baryon density. *Nucl. Phys. B*, 582:477–513, 2000.
- [21] Simon Hands, Seyong Kim, and Jon-Ivar Skullerud. Deconfinement in dense 2-color QCD. *Eur. Phys. J. C*, 48:193, 2006.
- [22] Tamer Boz, Pietro Giudice, Simon Hands, and Jon-Ivar Skullerud. Dense two-color QCD towards continuum and chiral limits. *Phys. Rev. D*, 101(7):074506, 2020.
- [23] V. V. Braguta, E. M. Ilgenfritz, A. Yu. Kotov, A. V. Molochkov, and A. A. Nikolaev. Study of the phase diagram of dense two-color QCD within lattice simulation. *Phys. Rev. D*, 94(11):114510, 2016.
- [24] N. Astrakhantsev, V. V. Braguta, E. M. Ilgenfritz, A. Yu. Kotov, and A. A. Nikolaev. Lattice study of thermodynamic properties of dense QC₂D. *Phys. Rev. D*, 102(7):074507, 2020.
- [25] Thomas Schäfer. Patterns of symmetry breaking in QCD at high baryon density. *Nucl. Phys. B*, 575:269–284, 2000.
- [26] Masanori Hanada and Naoki Yamamoto. Universality of Phases in QCD and QCD-like Theories. *JHEP*, 02:138, 2012.
- [27] Takuya Kanazawa, Tilo Wettig, and Naoki Yamamoto. Banks-Casher-type relation for the BCS gap at high density. *Eur. Phys. J. A*, 49:88, 2013.
- [28] Kei Iida, Etsuko Itou, Kotaro Murakami, and Daiki Suenaga. Hadron spectra of finite-density QC₂D. 6 2026.
- [29] Katsuya Ishiguro, Kei Iida, and Etsuko Itou. Flux tube profiles in two-color QCD at low temperature and high density. *PoS, LATTICE2021:063*, 2022.
- [30] A. Begun, V. G. Bornyakov, V. A. Goy, A. Nakamura, and R. N. Rogalyov. Study of two color QCD on large lattices. *Phys. Rev. D*, 105(11):114505, 2022.
- [31] D. T. Son and M. A. Stephanov. QCD at a finite isospin density: From the pion to quark-antiquark condensation. *Physics of Atomic Nuclei*, 64(5):834–842, may 2001.
- [32] Simon Hands, Seyong Kim, Dale Lawlor, Andrew Lee-Mitchell, and Jon-Ivar Skullerud. Dense QC₂D: What’s up with that?!? *PoS, LATTICE2024:165*, 2025.
- [33] Bastian B. Brandt, Francesca Cuteri, and Gergely Endrodi. Equation of state and speed of sound of isospin-asymmetric QCD on the lattice. *JHEP*, 07:055, 2023.
- [34] Ryan Abbott, William Detmold, Fernando Romero-López, Zohreh Davoudi, Marc Illa, Assumpta Parreño, Robert J. Perry, Phiala E. Shanahan, and Michael L. Wagman. Lattice quantum chromodynamics at large isospin density. *Phys. Rev. D*, 108(11):114506, 2023.

- [35] Ryan Abbott, William Detmold, Marc Illa, Assumpta Parreño, Robert J. Perry, Fernando Romero-López, Phiala E. Shanahan, and Michael L. Wagman. QCD Constraints on Isospin-Dense Matter and the Nuclear Equation of State. *Phys. Rev. Lett.*, 134(1):011903, 2025.
- [36] Eemeli Annala, Tyler Gorda, Joonas Hirvonen, Oleg Komoltsev, Alekski Kurkela, Joonas Nättilä, and Alekski Vuorinen. Strongly interacting matter exhibits deconfined behavior in massive neutron stars. *Nature Commun.*, 14(1):8451, 2023.
- [37] Larry McLerran and Sanjay Reddy. Quarkyonic Matter and Neutron Stars. *Phys. Rev. Lett.*, 122(12):122701, 2019.
- [38] Toru Kojo. Stiffening of matter in quark-hadron continuity. *Phys. Rev. D*, 104(7):074005, 2021.
- [39] Jens Braun, Andreas Geißel, and Benedikt Schallmo. Speed of sound in dense strong-interaction matter. *SciPost Phys. Core*, 7:015, 2024.
- [40] Kenji Fukushima and Shuhei Minato. Speed of sound and trace anomaly in a unified treatment of the two-color diquark superfluid, the pion-condensed high-isospin matter, and the 2SC quark matter. *Phys. Rev. D*, 111(9):094006, 2025.